Soft Matter

View Online
Dynamic Article Links

Cite this: *Soft Matter*, 2011, **7**, 5188

www.rsc.org/softmatter

PAPER

Bending and twisting of soft materials by non-homogenous swelling

Douglas P. Holmes,* Matthieu Roché, Tarun Sinha and Howard A. Stone

Received 14th December 2010, Accepted 22nd March 2011
DOI: 10.1039/c0sm01492c

Soft materials such as biological tissues and gels undergo morphological changes, motion, and instabilities when subjected to external stimuli. We examine how thin elastic plates undergo rapid bending and buckling instabilities after non-homogenous exposure to a favorable solvent that swells the network. An unconstrained beam bends along its length, while a circular disc bends and buckles with multiple curvatures. In the case of a disc, a large-amplitude transverse travelling wave rotates azimuthally around the disc. We provide theoretical interpretations inspired by the complementary thermal expansion problem of transient shape changes triggered by non-homogenous time-dependent heating, which allows collapse of time-dependent swelling data onto universal curves. Control of dynamical, swelling-induced shape changes provides new directions for the utilization of soft materials.

1 Introduction

Tissues can exhibit residual internal stresses induced by growth,[1–5] and generate elastic deformations to move in response to light or touch,[6–8] curl articular cartilage,[9] aid in seed dispersal,[10,11] and actuate hygromorphs, such as pine cones.[12] Understanding the dynamics of such osmotically driven movements and the influence of geometry and boundary conditions, is crucial to the controlled deformation of soft materials.[4,13–17] For example, the steady permeation of fluid through rigid porous networks[18] and the equilibrium swelling of crosslinked elastic networks are well studied.[19,20] A specific focus has been the equilibrium shapes that hydrogels adopt under a prescribed state of stress.[4,21] Research has also focused on the kinetics of swelling of soft elastomers and gels[16,22–24] and the relaxation of gels during bending[25] and indentation.[26] Very recently, several papers have focused on coupling equilibrium swelling information with dynamic deformations for liquid crystal elastomers, rubber, and paper.[27–30] In this paper, we study the impact of material geometry and non-homogenous swelling on the dynamics of deformation of soft materials.

We present the time-dependent shape changes and dynamic instabilities that occur by non-homogenously swelling an elastomer. In particular, we examine the dynamics as thin elastic plates undergo rapid bending (Fig. 1a) when swollen with a favorable solvent (*e.g.* hexane [hex], silicone oil [Si]). The material recovers its original shape at longer times when the solvent has spread uniformly throughout the sample; at much longer times the solvent may evaporate, as in the case of hexane, to leave a uniform solvent-free state. While uniform swelling of a beam leads to a well-studied global deformation,[19,20,25] large deformations can also occur over small regions of the beam in response to localized stimuli. For example, a beam swollen at spatially distributed locations on the top and bottom surfaces adopts an *s*-shape (Fig. 1b). The inverse is also possible, as solvent-induced swelling can flatten an initially curved beam (Fig. 1c). Developing a quantitative description of the magnitude and timescale of the deformation of soft materials will be important for understanding of the dynamics of morphogenesis in growing soft tissues,[3] and will contribute to the technology of advanced elastic materials for stretchable electronics, soft robotics, adaptable shape change, and the direction and control of fluid flow.

2 Bending of a slender beam

2.1 Non-homogenous swelling of a quasi one-dimensional beam

First, we study the time-dependence for the simplest case of a slender beam in response to a non-homogenous strain (Fig. 1a). The top surface of a crosslinked polydimethylsiloxane (PDMS) beam with thickness h and length L was swollen with a favorable solvent by placing a small drop (30 μL) at the center of the beam. Bending is characterized by the radius of curvature R, or its inverse κ_1, measured at the midpoint of the centerline (Fig. 1d). Equilibrium swelling causes the elastomer to expand to an experimentally measured maximum strain, $\varepsilon_m \approx 0.2$–$0.3$, which is consistent with values reported in the literature.[20] In our experiments, the drop rapidly spreads over the top surface and slowly is absorbed into the elastomer. As the top of the beam expands the remainder of the beam is required to bend to accommodate this deformation. The beam bends as the fluid permeates through the thickness of the beam until it reaches a maximum curvature when the imbibition front has reached the approximate centerline, after which the beam relaxes, slowly bending back to its original shape.

Department of Mechanical and Aerospace Engineering, Princeton University, G02 Engineering Quad, Olden St., Princeton, NJ, USA. E-mail: dpholmes@princeton.edu; Tel: +01 609 258 9015

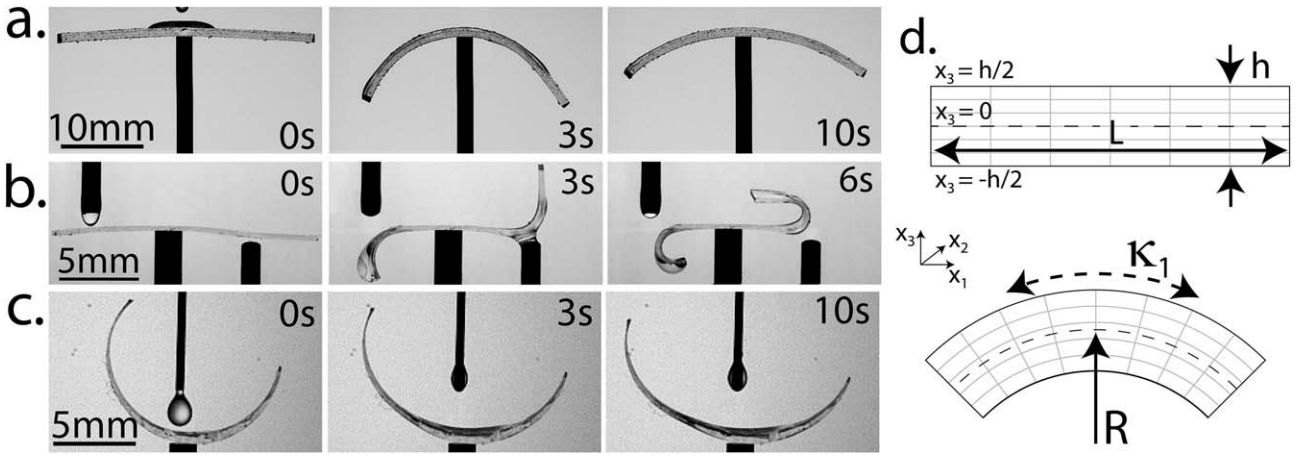

Fig. 1 Global and localized bending of beams swollen non-homogenously with a favorable solvent. *a.* A narrow beam ($h \approx 1$ mm, $w \approx 0.5$ mm, $L \approx 20$ mm) with free edges is swollen non-homogenously by placing a droplet of hexane on one side. The expansion of the top surface of the beam causes the material to initially bend sharply and then relax back to its initial shape. *b.* A beam swollen with hexane at two locations on opposite faces leads to localized bending of opposite curvatures. *c.* An initially curved beam bends and decreases its curvature when swollen with a favorable solvent. *d.* A schematic of a beam expanding and subsequently bending, with definitions of the geometric variables for describing the deformations.

We measured the average curvature of the centerline of the beam as a function of time (Fig. 2 a, b) for samples of various thickness and using two different solvents with different viscosities ($\mu_{hex} = 0.3$ *cSt* and $\mu_{Si} = 1$ *cSt*) that swell PDMS.[20] The qualitative features of the dynamics are the same for beams of varying thickness and different fluid properties. The raw data from Fig. 2b illustrates that experiments span several orders of magnitude in timescale and nearly an order of magnitude in curvature for the fluids and thicknesses studied. It is important to note that solvent evaporation occurs over a timescale longer than the deformation dynamics presented, *i.e.* the dynamics from swelling with hexane occur within 1–2 s, while evaporation of the same volume of solvent occurs over $\simeq$ 30 s. This evaporation occurs over a longer time when the solvent is within the elastomeric network.

2.2 Analogy to thermal bending of beams

To understand these trends produced by non-homogenous swelling of an elastomer, it is helpful to draw an analogy to the thermal bending of beams, *e.g.* time-dependent bending by heating a narrow beam on one side ($x_3 = h/2$) with temperature

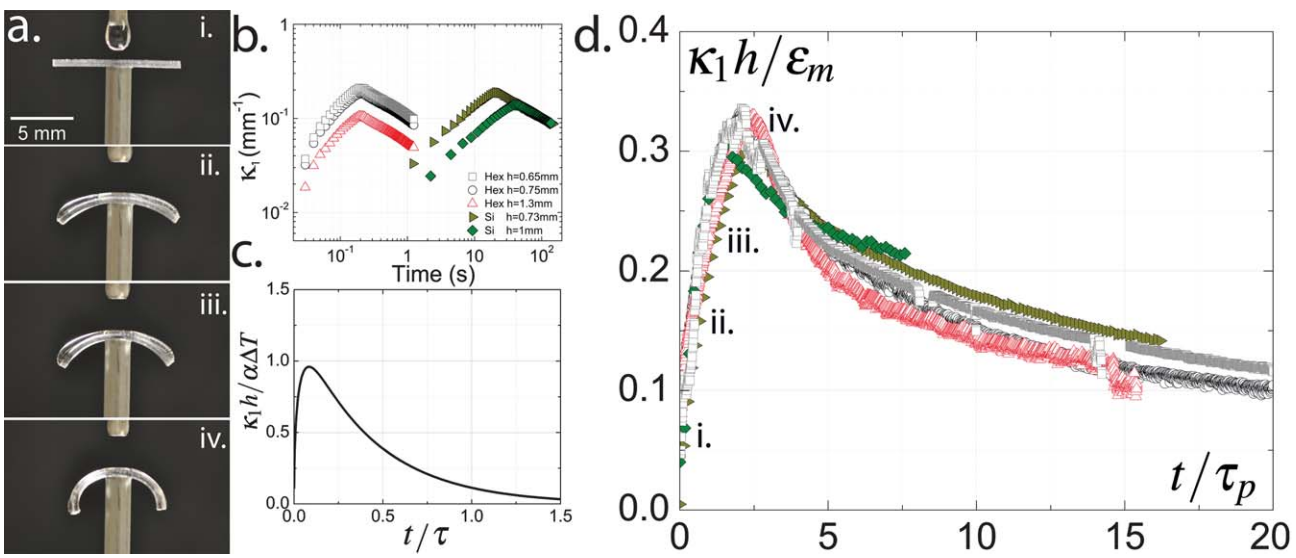

Fig. 2 Dynamics of beam bending. *a.* Images of a beam swollen with silicone oil ($h = 1$ mm) bending to its maximum curvature. *b.* Raw data of curvature *versus* time for beams of various thicknesses swollen with different solvents. *c.* A plot of normalized beam curvature, $\frac{\kappa_1 h}{\varepsilon_m(1+\nu)}$, *versus* time normalized by the diffusion time, τ, based on the analogy with the thermal bending of beams. *d.* The raw data from *b* is normalized based on the parameters in eqn (4), with time scaled by the poroelastic time, τ_p. The data for a range of beam thicknesses and fluid properties collapses to a qualitatively similar profile that is predicted by eqn (4).

increment,[31–33] ΔT. The time scale, τ, for the swelling front to propagate across the beam is h^2/D, where D is the characteristic diffusivity. This analogy is useful due to the empirically observed diffusive-like nature of the fluid imbibing into the elastomer.[16] The thermal gradient is determined by the unsteady, transverse diffusion of temperature, T, from the top surface of a beam, $D\frac{\partial^2 T}{\partial x_3^2} = \frac{\partial T}{\partial t}$, where x_3 is the transverse dimension. Assuming the bottom surface of the beam is perfectly insulating, the temperature distribution is:

$$\frac{T}{\Delta T} = 1 - \sum_{n=0}^{\infty} \frac{2}{\lambda_n} \sin\left[\lambda_n\left(\frac{1}{2} - \frac{x_3}{h}\right)\right] e^{-\lambda_n^2 t/\tau}, \quad (1)$$

where $\lambda_n = \frac{(2n+1)\pi}{2}$. We treat the beam as a slender body, and assume that the dominant strains are along the x_1 axis, and relate the swelling induced bending moment to the curvature, κ_1, which yields:

$$\kappa_1 = \frac{12}{h^3}\int_{-h/2}^{h/2} \varepsilon_1(x_3) x_3 dx_3, \quad (2)$$

where $O(1)$ factors of the Poisson's ratio have been neglected since these depend on details of the transverse strain distribution. Using the diffusion of temperature to calculate the thermally induced strain, $\alpha\Delta T$, where α is the thermal expansion coefficient, the normalized beam curvature becomes:

$$\frac{\kappa_1 h}{\alpha \Delta T} = -12 \sum_{n=0}^{\infty} e^{-\lambda_n^2 t/\tau}\left(\frac{\lambda_n - 2(-1)^n}{\lambda_n^3}\right). \quad (3)$$

The first few terms for the curvature from this calculation are:

$$\frac{\kappa_1 h}{\varepsilon_m} = 1.33 e^{-\frac{\pi^2 t/\tau}{4}} - 0.770 e^{-\frac{9\pi^2 t/\tau}{4}} + \ldots \quad (4)$$

where the maximum strain is $\varepsilon_m = \alpha\Delta T$ for this thermal analogy, and the expression for κ_1 is expected to be valid for times not too small. The two exponentials dictate that the beam will bend rapidly to a maximum curvature on the time scale τ, before slowly bending back to its original, flat shape. The normalized beam curvature is plotted as a function of t/τ in Fig. 2c.

In the case of our swelling experiments with an elastic gel, the effective diffusivity[22] is $D \approx Ek/\mu$, where E is the elastic modulus ($E = 10^6$ Pa) and k is the permeability of the material[34] ($k \approx 10^{-18}$ m^2 s^{-1}). These quantities define the poroelastic time:

$$\tau_p = \mu h^2/kE. \quad (5)$$

The normalized beam curvature, $\kappa h/\varepsilon_m$ is plotted *versus* t/τ_p, in Fig. 2d, which demonstrates how the non-homogenous swelling dynamics can be collapsed across several orders of magnitude in time and curvature. The beam rapidly reaches its maximum curvature, κ_{max} at a time $\approx 2\tau_p$, while the relaxation occurs slowly, qualitatively similar to the thermal response indicated in eqn (4). Relaxation for samples swollen with hexane occurs slightly faster than for the silicone oils, which we believe is due to evaporation of the solvent, which is negligible for the silicone oils over these time scales. Since ε_m, the maximum strain in the elastic gel, is obtained from long-time equilibrium measurements, this likely overestimates the strain in the partially swollen beam, which rationalizes why the data in Fig. 2d has a vertical scale less than unity. It is important to note that the thermal analogy is only presented to provide a qualitative description of our dynamical phenomena and a rational introduction for scaling the data to produce collapse onto a universal curve. Thermal equilibrium in a metal is reached instantaneously (*i.e.* thermal expansion is caused by a change in interatomic distance) while the timescale for a gel or elastomer to reach equilibrium is much slower. Consequently, a quantitative collapse between the two phenomena should not be expected.[16]

3 Circular discs

3.1 Bending and bifurcation

Having developed an understanding of the dynamic response for a quasi-one-dimensional beam in response to non-homogenous strain, we studied the dynamics of a quasi-two-dimensional geometry, *i.e.* a circular disc. The discs of thickness h and radius a are initially axisymmetric, and their deformation at any instant is characterized by two principle curvatures, κ_1 and κ_2, which are measured orthogonal to each other *via* image analysis. A drop of hexane placed on the surface of a circular disc spreads rapidly and causes the disc to swell and bend. First, we report the time-dependence of the curvatures by scaling time with τ_p. Upon swelling, the disc initially bends with $\kappa_1 = \kappa_2$ (Fig. 3 a-i and ii). As swelling continues, a bifurcation occurs and the principle curvatures become unequal with one growing in magnitude and the other decreasing (Fig. 3 a and b). Following the bifurcation, the orientations of the principle curvature axes change continually in time, as discussed below. At long times the disc recovers its equilibrium flat shape.

The experimental shapes of bifurcated circular discs presented in this paper can be explained *via* the von Kármán plate theory, which predicts that a disc subjected to a strain gradient along the x_3 direction buckles symmetrically before bifurcating into two positive, but distinct curvatures.[33,35] By continuing the analogy with the thermal swelling and bending of a beam discussed above, the approximate shape of a plate is described by two curvatures, κ_1 and κ_2, with mid-plane displacements in the principle directions of:

$$u_1 = A_1 x_1 + A_2 x_1^3 + A_3 x_1 x_2^2 \quad (6a)$$

$$u_2 = B_1 x_2 + B_2 x_2^3 + B_3 x_2 x_1^2 \quad (6b)$$

$$u_3 = \frac{\kappa_1 x_1^2}{2} + \frac{\kappa_2 x_2^2}{2}, \quad (6c)$$

where A_i and B_i are six parameters selected to minimize the potential energy of the plate[33,35] The complexity in coupling the spatial and temporal parameters for the axisymmetric circular disc makes it difficult to solve the von Kármán plate equations for both short times, $\frac{t}{\tau} \ll 1$, and long times, $\frac{t}{\tau} \gg 1$. In order to capture the most significant qualitative features of the time-dependent response in the experiments, *e.g.* the bifurcation and slow relaxation, we approximate the thermal strains by a simple function, $f(t/\tau) \approx A\frac{t}{\tau} e^{-B\sqrt{\frac{t}{\tau}}}$, which represents the beam

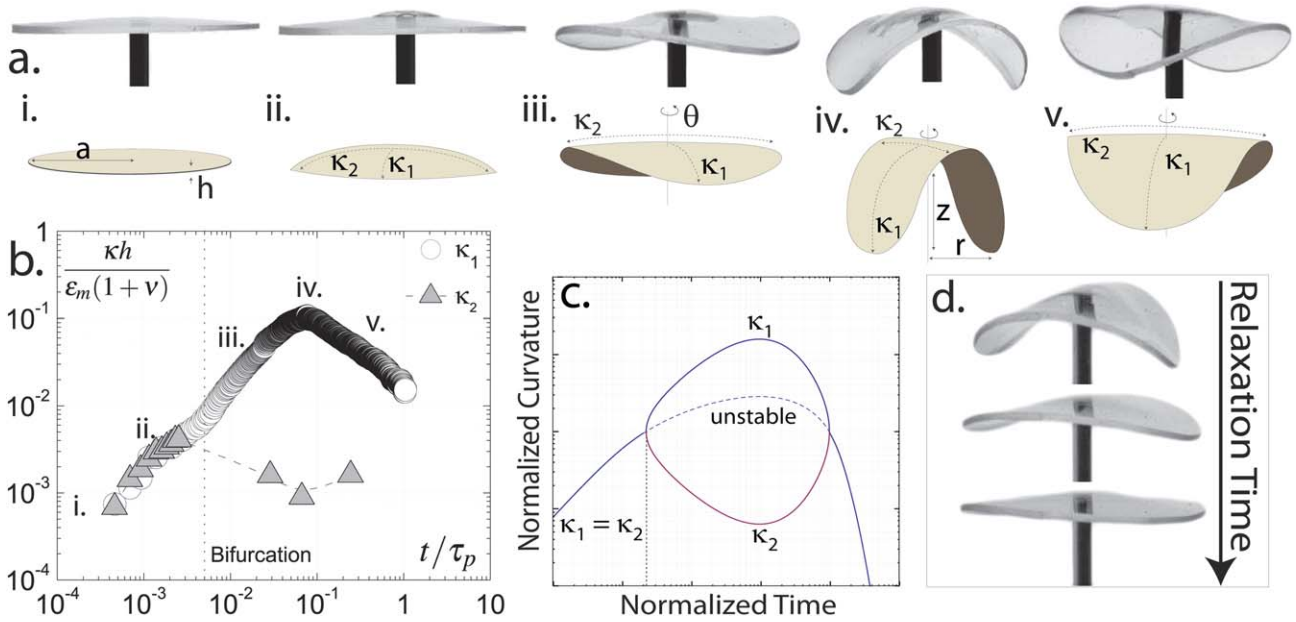

Fig. 3 Bending and bifurcation of circular discs. *a*. Optical images and schematic as a circular disc buckles axisymetrically, *i.e.* $\kappa_1 = \kappa_2$, before bifurcating with two distinct, positive curvatures $\kappa_1 \neq \kappa_2$. *b*. A plot of normalized disc curvature *versus* time for a circular disc non-homogenously swollen with hexane. A bifurcation occurs causing the two curvatures to differ in magnitude (dashed line added to guide the eye). *c.* Normalized curvature *vs.* normalized time is determined by minimizing the total strain energy of the disc. Our experimental data is in very good agreement with this theory. *d.* Images of the circular disc as it relaxes back to its initial, flat state.

response in Fig. 2c for all $\frac{t}{\tau}$, where $A = 27$ and $B = 6.5$. Then, minimizing the total strain energy for the disc leads to two algebraic equations describing the principle curvatures:

$$\kappa_1 h\nu + \kappa_2 h\left[1 - (a/2h)^4(\kappa_1 h)^2(\nu^2 - 1)\right] + \frac{\varepsilon_m}{16}(1+\nu)f(t/\tau) = 0 \quad (7)$$

$$\kappa_2 h\nu + \kappa_1 h\left[1 - (a/2h)^4(\kappa_2 h)^2(\nu^2 - 1)\right] + \frac{\varepsilon_m}{16}(1+\nu)f(t/\tau) = 0 \quad (8)$$

where a is the disc radius, and ν is Poisson's ratio.[35] When solving for the principle curvatures as a function of time, three regimes emerge (Fig. 3c): *i*. Below a bifurcation strain the disc bends axisymmetrically ($\kappa_1 = \kappa_2$), similar to a hemispherical lens, then *ii*. above a bifurcation strain, two different, positive curvatures exist, and *iii*. at long time, when the entire system approaches an isothermal state, the disc relaxes back to the initial, flat state (κ_1,$\kappa_2 \rightarrow 0$). We present a qualitative plot of the curvatures as a function of the normalized time from this thermal analogy in Fig. 3c. Our experimental observations (Fig. 3b), including bending, the bifurcation, and slow relaxation, are in excellent qualitative agreement with the time-dependent thermal analogy for the bending and buckling of a circular disc.

3.2 Twisting: propagation of an azimuthal buckle wave

As indicated above, after the disc bifurcates, generating two different curvatures, the orientations of the principle axes rotate azimuthally around the disc. Fig. 4a shows a top-view of a swollen, buckled circular disc with a shape that appears to rotate in a clockwise manner. As the buckle rotates, the material points do not translate in the azimuthal direction. To emphasize that the disc experiences deformation in the form of a travelling wave and only deforms in the vertical direction during the dynamic buckle rotation, we mark several points on the disc with small pins and observe their displacements (Fig. 4b). The disc remains symmetric about its two principle curvatures, as shown in Fig. 4c, where we plot the position of two points on the disc initially separated by $\theta = \pi$ as a function of time. Buckle rotation begins to occur approximately when the critical strain for bifurcation is reached and increases until κ_1 reaches a maximum curvature. The directionality of this rotation appears arbitrary across numerous experiments. For example, Fig. 4d-i shows θ *versus* time plots for the dynamics to illustrate that the travelling wave can rotate entirely in one direction, the opposite direction, or back-and-forth (Fig. 4d-ii).

To the best of our knowledge, experimental observation of this buckle rotation instability is new and will require further investigation, both experimentally and theoretically to understand and make predictions about the phenomenon. Existence of disc rotation due to the nonlinear deformation of a disc with a differential strain across its thickness has been predicted numerically by Freund.[35] To rationalize that the second buckling mode, where $\kappa_1 \neq \kappa_2$, has no preferential configuration, we note that there are numerous orientations of the two principle curvatures that are energetically favorable. Any perturbation may cause the azimuthal shape of the disc to undergo reorientations to other energetic minima. Freund noted that a small difference in strain between the x_1 and x_2 directions can induce stable deformation beyond the point of bifurcation.[35] In our experiments, due to the dynamics of imbibition and swelling,

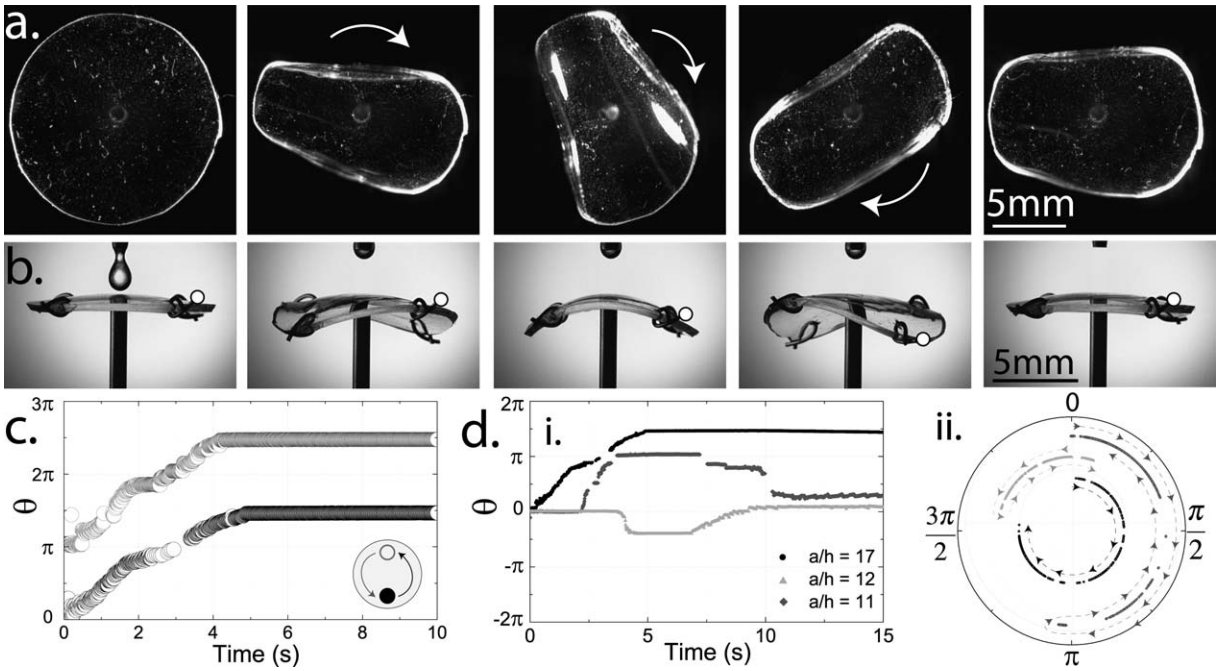

Fig. 4 Twisting of circular discs *a*. The formation of unstable buckling modes causes a travelling wave to propagate around the disc. Images from the top of a disc show it twisting clockwise. *b*. Images of a marked disc (enhanced with points to guide the eye) illustrate the movements of a fixed point on the disc. *c*. A plot of the position of two points on a disc initially separated by $\theta = \pi$ as a function of time. The disc is symmetric during buckle rotation. *d. i*. A plot of θ *versus* time and *ii*. θ in polar coordinates illustrates the disc's arbitrary directionality.

solvent continues to permeate vertically and laterally within the disc. The mechanical coupling between stress and the amount of solvent absorbed may lead to a perturbation, or mismatch strain, significant enough to cause a travelling buckle wave to propagate azimuthally around the disc.

4 Conclusions

In conclusion, we have presented a study on the dynamical deformation of soft materials in response to non-homogenous strains produced by swelling the material with a favorable solvent. We have shown how controlled, reversible shape changes are possible. Using an analogy with the thermal bending of beams and discs, we qualitatively describe the time-dependent deformation. The theory provides normalized parameters for the curvature dynamics and the typical timescales. For the case of a circular disc, the theory captures the bifurcation and relaxation that occurs when multiple curvatures are accessible. Upon bifurcation, a rotating buckle wave was observed with an arbitrary direction, which is a new dynamical phenomenon that requires further experimental and theoretical study across a variety of materials and geometries. Although recent investigations of osmotically swollen materials have concerned the material's final equilibrium shape, our observations, in particular the rotation travelling wave on a disc, emphasize the importance of the dynamical pathways and potential instabilities that have not previously been considered. Further exploration of the dynamics of stressed, elastic materials, as introduced here in unconstrained geometries, should be of significant importance in fields ranging from morphogenesis to adaptable smart materials, and future studies should also incorporate the effects of confinement.

Experimental section

PDMS preparation and swelling

A 10 : 1 (w/w) degassed mixture of polydimethylsiloxane (Sylgard 184^{TM}) prepolymer and curing agent was molded into slender beams ($w \simeq 0.5$ mm) and circular discs ($E = 1$ MPa, $\nu \approx 0.5$) of various length and thickness, and crosslinked at 65 °C overnight. The PDMS films were placed on, but not adhered to, metal posts with a diameter of 1.7 mm. The ability for the free-standing elastomer to deform equally when swollen from above and below, as shown in Fig. 1b, indicates that the post it rests on has no quantifiable impact on the local curvatures. The solvents hexane and silicone oil were chosen due to their nearly identical thermodynamic solubility parameter to PDMS:[20] $\delta \approx 7.3$ cal$^{1/2}$ cm$^{-3/2}$. A droplet ($V = 30$ μL) of either hexane (Sigma-Aldrich) or silicone oil (Sigma-Aldrich), was placed on the top surface of the PDMS film *via* a Harvard Apparatus PHD 2000 syringe pump.

Imaging and characterization

The deformation of the slender beams swollen with hexane was imaged with a Phantom V7.3 high-speed camera with a macro lens ($f = 105$ mm) at 100 f ps. Slender beams swollen with silicone oil were imaged using a Nikon D90 and macro lens at 0.8 f ps. The deformation of the circular disc was imaged by two orthogonal high-speed cameras (Phantom V7.3 and Phantom V9 with macro lenses) at 100 f ps. Image analysis was performed

with ImageJ and custom Matlab code that isolated the object's shape, allowing the relevant curvatures to be measured as a function of time.

Acknowledgements

Funding for this work was provided by the Princeton Institute for the Science and Technology of Materials, the Princeton MRSEC, and the ARO MURI (#W911NF-09-1-0476). The authors acknowledge the helpful feedback from Ian Griffiths, Matthew Girardi, Paola Nardinocchi, and John Hutchinson; the latter suggested the idea that the rotating wave may be due to a coupling of stress and solvent absorption.

References

1 M. King, J. Vincent and W. Harris, *New Zealand Journal of Botany*, 1996, **34**, 411–416.
2 B. Moulia, *Journal of Plant Growth Regulation*, 2000, 19–30.
3 M. Ben Amar and A. Goriely, *J. Mech. Phys. Solids*, 2005, **53**, 2284–2319.
4 Y. Klein, E. Efrati and E. Sharon, *Science*, 2007, **315**, 1116–1120.
5 J. Dervaux and M. Ben Amar, *Phys. Rev. Lett.*, 2008, **101**, 068101.
6 J. Braam, *New Phytol.*, 2004, **165**, 373–389.
7 J. Skotheim and L. Mahadevan, *Science*, 2005, **308**, 1308–1310.
8 Y. Forterre, J. M. Skotheim, J. Dumais and L. Mahadevan, *Nature*, 2005, **433**, 421–425.
9 L. A. Setton, H. Tohyama and V. C. Mow, *J. Biomech. Eng.*, 1998, **120**, 355–61.
10 J. Edwards, D. Whitaker, S. Klionsky and M. J. Laskowski, *Nature*, 2005, **435**, 164.
11 R. Elbaum, L. Zaltzman, I. Burgert and P. Fratzl, *Science*, 2007, **316**, 884–6.
12 E. Reyssat and L. Mahadevan, *J. R. Soc. Interface*, 2009, **6**, 951–7.
13 T. Tanaka, S. T. Sun, Y. Hirokawa, S. Katayama, J. Kucera, Y. Hirose and T. Amiya, *Nature*, 1987, **325**, 796–798.
14 W. T. S. Huck, N. Bowden, P. Onck, T. Pardoen, J. W. Hutchinson and G. M. Whitesides, *Langmuir*, 2000, **16**, 3497–3501.
15 A. Boudaoud, E. Hamm and F. Melo, *Phys. Rev. Lett.*, 2007, **99**, year.
16 M. Doi, *J. Phys. Soc. Jpn.*, 2009, **78**, 052001.
17 D. Holmes and A. Crosby, *Phys. Rev. Lett.*, 2010, **105**, 038303.
18 M. Biot, *J. Appl. Phys.*, 1941, **12**, 155–164.
19 P. Flory, *Principles of Polymer Chemistry*, Cornell University Press, Ithaca, NY, 1953, pp. 581–584.
20 J. N. Lee, C. Park and G. M. Whitesides, *Anal. Chem.*, 2003, **75**, 6544–54.
21 T. Mora and A. Boudaoud, *Eur. Phys. J. E*, 2006, **20**, 119–24.
22 T. Tanaka and D. Fillmore, *J. Chem. Phys.*, 1979, **79**, 1214–1218.
23 Y. Li and T. Tanaka, *J. Chem. Phys.*, 1990, **92**, 1365.
24 T. Yamaue and M. Doi, *Phys. Rev. E: Stat., Nonlinear, Soft Matter Phys.*, 2004, **69**, 1–5.
25 G. W. Scherer, J. H. Prévost and Z.-H. Wang, *Int. J. Solids Struct.*, 2009, **46**, 3451–3462.
26 Y. Hu, X. Zhao, J. J. Vlassak and Z. Suo, *Appl. Phys. Lett.*, 2010, **96**, 121904.
27 Y. Sawa, K. Urayama, T. Takigawa, A. DeSimone and L. Teresi, *Macromolecules*, 2010, **43**, 4362–4369.
28 S. Douezan, M. Wyart, F. Brochard-Wyart and D. Cuvelier, *Soft Matter*, 2011, **7**, 1506.
29 C. Nah, G. Lee, C. Lim, J. Ahn and A. Gent, *Macromolecules*, 2011, 783–789.
30 E. Reyssat and L. Mahadevan, *Europhys. Lett.*, 2011, **93**, 54001.
31 L. Rayleigh, *Philos. Mag., Ser. 5*, 1901, **1**, 169–178.
32 S. Timoshenko, *J. Opt. Soc. Am.*, 1925, **11**, 233.
33 A. Bower, *Applied Mechanics of Solids*, CRC Press, 2009.
34 *Polymer Data Handbook*, ed. J. Mark, Oxford University Press, Oxford, 1999.
35 L. Freund, *J. Mech. Phys. Solids*, 2000, **48**, 1159–1174.